Inorg. Chem. **2006**, *45*, 967–976

Understanding the Origin of Metal–Sulfur Vibrations in an Oxo-Molybdenum Dithiolene Complex: Relevance to Sulfite Oxidase

Frank E. Inscore,[†] Sushilla Z. Knottenbelt,[‡] Nick D. Rubie,[‡] Hemant K. Joshi,[†] Martin L. Kirk,*[,‡] and John H. Enemark*[,†]

Department of Chemistry, University of Arizona, Tucson, Arizona 85721, and Department of Chemistry, The University of New Mexico, MSC03 2060, 1 University of New Mexico, Albuquerque, New Mexico 87131-0001

Received May 3, 2005

X-ray crystallography and resonance Raman (rR) spectroscopy have been used to further characterize (Tp*)MoO(qdt) (Tp* is hydrotris(3,5-dimethyl-1-pyrazolyl)borate and qdt is 2,3-quinoxalinedithiolene), which represents an important benchmark oxomolybdenum mono-dithiolene model system relevant to various pyranopterin Mo enzyme active sites, including sulfite oxidase. The compound (Tp*)MoO(qdt) crystallizes in the triclinic space group, $P\bar{1}$, where $a = 9.8424$ (7) Å, $b = 11.2323$ (8) Å, $c = 11.9408$ (8) Å, $\alpha = 92.7560$ (10)°, $\beta = 98.9530$ (10)°, and $\gamma = 104.1680$ (10)°. The (Tp*)MoO(qdt) molecule exhibits the distorted six-coordinate geometry characteristic of related oxo-Mo(V) systems possessing a single coordinated dithiolene ligand. The first coordination sphere bond lengths and angles in (Tp*)MoO(qdt) are very similar to the corresponding structural parameters for (Tp*)MoO(bdt) (bdt is 1,2-benzenedithiolene). The relatively small inner-sphere structural variations observed between (Tp*)MoO(qdt) and (Tp*)MoO(bdt) strongly suggest that geometric effects are not a major contributor to the significant electronic structural differences reported for these two oxo-Mo(V) dithiolenes. Therefore, the large differences observed in the reduction potential and first ionization energy between the two molecules appear to derive primarily from differences in the effective nuclear charges of their respective sulfur donors. However, a subtle perturbation to Mo–S bonding is implied by the nonplanarity of the dithiolene chelate ring, which is defined by the fold angle. This angular distortion ($\theta = 29.5°$ in (Tp*)MoO(qdt); 21.3° in (Tp*)MoO(bdt)) observed between the MoS_2 and S–C═C–S planes may contribute to the electronic structure of these oxo-Mo dithiolene systems by controlling the extent of S p–Mo d orbital overlap. In enzymes, the fold angle may be dynamically modulated by the pyranopterin, thereby functioning as a transducer of vibrational energy associated with protein conformational changes directly to the active site via changes in the fold angle. This process could effectively mediate charge redistribution at the active site during the course of atom- and electron-transfer processes. The rR spectrum shows bands at 348 and 407 cm^{-1}. From frequency analysis of the normal modes of the model, $[(NH_3)_3MoO(qdt)]^{1+}$, using the Gaussian03 suite of programs, these bands are assigned as mixed-mode Mo–S vibrations of the five-membered Mo-ditholene core structure. Raman spectroscopy has also provided additional evidence for an in-plane pseudo-σ dithiolene S–Mo d_{xy} covalent bonding interaction in (Tp*)MoO(qdt) and related oxo-Mo-dithiolenes that has implications for electron-transfer regeneration of the active site in sulfite oxidase involving the pyranopterin dithiolene.

Introduction

The pyranopterin molybdenum enzymes are categorized into three distinct families on the basis of structure and reactivity. These are referred to as the xanthine oxidase, sulfite oxidase, and DMSO reductase families, and they function to catalyze a variety of two-electron redox reactions coupled to a formal oxygen atom transfer between substrate and the active site.[1] The X-ray crystal structures for numerous members in each of these families have now been reported,[2–17]

* To whom correspondence should be addressed. E-mail: mkirk@unm.edu(M.L.K.); jenemark@u.arizona.edu (J.H.E.).
[†] University of Arizona.
[‡] The University of New Mexico.

(1) Hille, R. *Chem. Rev.* **1996**, *96* (7), 2757−2816.
(2) Czjzek, M.; Santos, J.-P. D.; Pomier, J.; Giordano, G.; Méjean, V.; Haser, R. *J. Mol. Biol.* **1998**, *284* (2), 435−447.

10.1021/ic0506815 CCC: $33.50 © 2006 American Chemical Society
Published on Web 01/11/2006

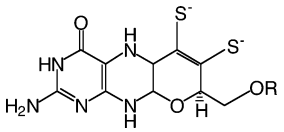

Figure 1. Structure of the pyranopterin−dithiolene cofactor derived from protein crystallographic studies.[2−17]

and a common active-site structural feature is coordination of the Mo atom by at least one pyranopterin−dithiolene (Figure 1).[18] The postulated roles of the pyranopterin−dithiolene include coupling the Mo redox center into efficient pyranopterin-mediated superexchange pathways for facilitating electron-transfer (ET) regeneration of the Mo resting state active site following formal oxygen atom transfer, modulating the Mo reduction potential, and transferring vibrational energy associated with protein conformational changes directly to the active site.[1,19−21]

The consensus active-site geometries of sulfite oxidase derived from X-ray crystallography,[3] X-ray absorption, and other spectroscopic studies[22−24] during the catalytic cycle are depicted in Figure 2. During enzymatic turnover, the mononuclear Mo center of sulfite oxidase (SO) is proposed to cycle

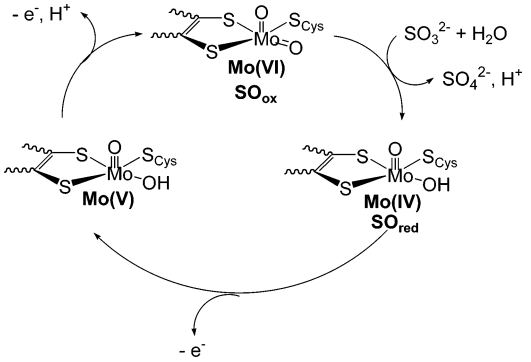

Figure 2. Structures representative of all three oxidation states in the catalytic cycle of SO.

between the Mo(VI) and Mo(IV) oxidation states, with the paramagnetic Mo(V) state being an obligatory catalytic intermediate in the oxidative half-reaction of the enzyme. The geometry of the catalytically competent five-coordinate Mo(VI) active site in oxidized chicken liver sulfite oxidase is approximately square pyramidal, with a terminal oxo ligand in the axial position and the four basal ligand positions occupied by two sulfur donor atoms from the dithiolene portion of the pyranopterin, a third sulfur donor atom from a cysteine residue, and a second terminal oxo ligand with direct access to substrate (sulfite) via a solvent access channel.[3] The protein backbone precludes accessibility by substrate to the unoccupied sixth coordination site trans to the apical oxo.[32] Although the crystallographically determined structure has been interpreted as being partially reduced from the oxidized Mo(VI) resting state to either Mo(V) or Mo(IV), a $[Mo^{VI}O_2]^{2+}$ active site in chicken liver SO has been confirmed by XAS on oxidized polycrystalline SO.[23] This description is also consistent with resonance Raman (rR) enhancement of both Mo═O stretches in fully oxidized recombinant human SO.[25] In the course of substrate oxidation, the Mo center is reduced from Mo(VI) to Mo(IV) in a concerted two-electron atom-transfer event, which constitutes the reductive half-reaction of the catalytic sequence. Formal oxygen atom transfer (OAT) results in a reduced mono-oxo Mo(IV) site with the apical Mo≡O bond oriented normal to the dithiolene plane and either H_2O or OH^- in the equatorial position that was occupied by a terminal oxo in SO_{ox}. The geometric arrangement of a single terminal oxo oriented cis to the dithiolene plane in the electron-transfer half-reaction of all pyranopterin Mo en-

(3) Kisker, C.; Schindelin, H.; Pacheco, A.; Wehbi, W.; Garrett, R.; Rajagopalan, K.; Enemark, J.; Rees, D. *Cell* **1997**, *91* (7), 973−983.
(4) McAlpine, A. S.; McEwan, A. G.; Shaw, A. L.; Bailey, S. *J. Biol. Inorg. Chem.* **1997**, *2* (6), 690−701.
(5) Schindelin, H.; Kisker, C.; Hilton, J.; Rajagopalan, K. V.; Rees, D. C. *Science* **1996**, *272*, 1615−1621.
(6) Schneider, F.; Löwe, J.; Huber, R.; Schindelin, H.; Kisker, C.; Knäblein, J. *J. Mol. Biol.* **1996**, *263* (1), 53−69.
(7) Romao, M.; Archer, M.; Moura, I.; Moura, J.; LeGall, J.; Engh, R.; Schneider, M.; Hof, P.; Huber, R. *Science* **1995**, *270* (5239), 1170−1176.
(8) Huber, R.; Hof, P.; Duarte, R. O.; Moura, J. J. G.; Moura, I.; Liu, M.-Y.; LeGall, J.; Hille, R.; Archer, M.; Romão, M. J. *Proc. Natl. Acad. Sci. U.S.A. − Biochemistry* **1996**, *93* (17), 8846−8851.
(9) Truglio, J.; Theis, K.; Leimkuhler, S.; Rappa, R.; Rajagopalan, K.; Kisker, C. *Structure* **2002**, *10* (1), 115−125.
(10) Li, H.-K.; Temple, C.; Rajagopalan, K. V.; Schindelin, H. *J. Am. Chem. Soc.* **2000**, *122* (32), 7673−7680.
(11) Boyington, J. C.; Gladyshev, V. N.; Khangulov, S. V.; Stadtman, T. C.; Sun, P. D. *Science* **1997**, *275*, 1305−1308.
(12) Stewart, L.; Bailey, S.; Bennett, B.; Charnock, J.; Garner, C.; McAlpine, A. *J. Biol. Chem.* **2000**, *299*, 593.
(13) McAlpine, A.; McEwan, A.; Bailey, S. *J. Mol. Biol.* **1998**, *275* (4), 613−623.
(14) Dias, J. M.; Than, M. E.; Humm, A.; Huber, R.; Bourenkov, G. P.; Bartunik, H. D.; Bursakov, S.; Calvete, J.; Caldeira, J.; Carneiro, C.; Moura, J. J. G.; Moura, I.; Romão, M. J. *Structure* **1999**, *7*, 65−79.
(15) Enroth, C.; Eger, B.; Okamoto, K.; Nishino, T.; Nishino, T.; Pai, E. *Proc. Natl. Acad. Sci. U.S.A.* **2000**, *97* (20), 10723−10728.
(16) Rebelo, J.; Macieira, S.; Dias, J. M.; Huber, R.; Ascenso, C. S.; Rusnak, F.; Moura, J. J. G.; Moura, I.; Romão, M. J. *J. Mol. Biol.* **2000**, *297* (1), 135−146.
(17) Rebelo, J. M.; Dias, J. M.; Huber, R.; Moura, J. J. G.; Romao, M. J. *JBIC* **2001**, *6* (8), 791−800.
(18) Kirk, M. L.; Helton, M. E.; McNaughton, R. L. *The Electronic Structure and Spectroscopy of Metallo-Dithiolene Complexes*; John Wiley and Sons: Hoboken, NJ, 2004; Vol. 52, pp 111−212.
(19) Inscore, F. E.; McNaughton, R.; Westcott, B. L.; Helton, M. E.; Jones, R. M.; Dhawan, I. K.; Enemark, J. H.; Kirk, M. L. *Inorg. Chem.* **1999**, *38*, 1401−1410.
(20) Helton, M. E.; Kirk, M. L. *Inorg. Chem.* **1999**, *38* (20), 4384−4385.
(21) Helton, M. E.; Gebhart, N. L.; Davies, E. S.; McMaster, J.; Garner, C. D.; Kirk, M. L. *J. Am. Chem. Soc.* **2001**, *123*, 10389−10390.
(22) George, G. N.; Garrett, R. M.; Prince, R. C.; Rajagopalan, K. V. *J. Am. Chem. Soc.* **1996**, *118* (36), 8588−8592.
(23) George, G. N.; Pickering, I. J.; Kisker, C. *Inorg. Chem.* **1999**, *38* (10), 2539−2540.
(24) Cramer, S. P.; Gray, H. B.; Rajagopalan, K. V. *J. Am. Chem. Soc.* **1979**, *101* (10), 2772−2774.
(25) Garton, S. D.; Garrett, R. M.; Rajagopalan, K. V.; Johnson, M. K. *J. Am. Chem. Soc.* **1997**, *119* (10), 2590−2591.
(26) Dhawan, I. K.; Pacheco, A.; Enemark, J. H. *J. Am. Chem. Soc.* **1994**, *116* (17), 7911−7912.
(27) Dhawan, I. K.; Enemark, J. H. *Inorg. Chem.* **1996**, *35*, 4873−4882.
(28) Helton, M. E.; Pacheco, A.; McMaster, J.; Enemark, J. H.; Kirk, M. L. *J. Inorg. Biochem.* **2000**, *80*, 227−233.
(29) Cleland, W. E.; Barnhart, K. M.; Yamanouchi, K.; Collison, D.; Mabbs, F. E.; Ortega, R. B.; Enemark, J. H. *Inorg. Chem.* **1987**, *26* (7), 1017−1025.
(30) Westcott, B. L.; Gruhn, N. E.; Enemark, J. H. *J. Am. Chem. Soc.* **1998**, *120* (14), 3382−3386.
(31) Carducci, M. D.; Brown, C.; Solomon, E. I.; Enemark, J. H. *J. Am. Chem. Soc.* **1994**, *116*, 11856−11868.
(32) George, G. N.; William, E.; Cleland, J.; Enemark, J. H.; Smith, B. E.; Kipke, C. A.; Roberts, S. A.; Cramer, S. P. *J. Am. Chem. Soc.* **1990**, *112* (7), 2541−2548.

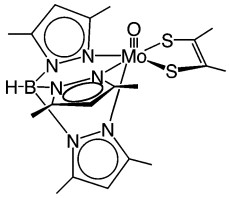

Figure 3. Basic stereochemistry of the [(Tp*)Mo^{V}O(dithiolene)] system showing the bidentate equatorial dithiolene ligands coordinated to the Mo center. The C_S effective coordination geometry in this system places the mirror plane coincident with the Mo≡O bond vector (directed along the *z* axis) and bisecting the MoN_2 and MoS_2 chelate angles defined by the N_2S_2 mean equatorial plane ($x-y$).

zymes has led to the "oxo-gate hypothesis".[18,19] The key concept here is that this geometry allows for significant in-plane coupling of the Mo d_{xy} redox orbital into efficient hole superexchange pathways for ET regeneration of the active catalyst.[19] Therefore, model complexes which possess a terminal oxo ligand oriented cis to the two sulfur donor atoms of an ene-1,2-dithiolate ligand represent the minimal structural feature of the Mo active site in SO and are important in furthering our understanding of geometric and electronic structure effects on ET reactivity. The regeneration of the resting Mo(VI) state in vertebrate SO constitutes the oxidative half-reaction, and this is accomplished by two sequential intramolecular one-electron processes from the Mo center to the endogenous *b*-type heme, where electrons are ultimately transferred to the physiological oxidant, cytochrome *c*. The one-electron, reduced Mo(V) intermediate is of particular interest and may be generated without the concomitant production of additional paramagnetic chromophores (i.e., low-spin ferric heme). This important catalytic intermediate has been probed in detail by EPR and MCD spectroscopies, providing considerable insight into the geometric and electronic structure of the site.[18,26−29]

The spectroscopic results on the Mo(V) states of sulfite oxidase have also provided impetus for synthesizing and characterizing a series of (Tp*)MoO(dithiolene) compounds,[19,20,26−36] including (Tp*)MoO(bdt) (**1**),[19,26,27] (Tp*)-MoO(tdt) (**2**),[19,29] (Tp*)MoO(bdtCl_2) (**3**),[34] and (Tp*)MoO-(qdt) (**4**).[20,33] The basic coordination geometry of these complexes is depicted in Figure 3. Until recently, complexes **1**−**4** were the only known oxo-Mo(V) species possessing a single dithiolene, and only **1** and **3** had been structurally characterized.[26,34] Holm and co-workers have now synthesized and characterized a number of Mo mono-dithiolene complexes, including those possessing a third sulfur donor (thiolate) ligand, that mimic the [Mo$^{VI}O_2$] and [Mo^{V}O] active-site structures of sulfite oxidase.[37] Recently, Kirk, Carrano, and co-workers have also synthesized and characterized new oxo-Mo monodithiolene models for SO_{red}.[38,39] Nonetheless, (Tp*)MoO(dithiolene) compounds remain important first-generation spectroscopic benchmarks for understanding the electronic structure of pyranopterin-containing molybdenum enzymes, especially xanthine oxidase and sulfite oxidase.[19,28,40] Previous detailed spectroscopic studies on (Tp*)MoO(bdt) (**1**) and (Tp*)MoO(qdt) (**4**) have shown how differences in the effective nuclear charges of the dithiolene sulfur donors can affect the inherent electronic structure of the corresponding (Tp*)MoO(dithiolene) complexes.[20,34,41] Recent reviews reveal the need for additional spectroscopic studies of well-defined model compounds that can provide insight for interpreting the complex vibrational spectra of molybdenum enzymes.[18,42] Complexes **1** and **4** possess very different dithiolene donor ligands. The quinoxolene ring in qdt is highly electron withdrawing, and this results in the qdt sulfurs being markedly poorer donors compared to the dithiolene sulfurs in bdt. The ligand donor ability has been used to explain the higher first ionization energy observed for Tp*MoO(qdt) compared to Tp*MoO-(bdt) and the fact that the former is ∼300 mV easier to reduce.[33] Here we determine the relationship between electronic and geometric structure in oxo-molybdenum dithiolenes and further elucidate how the dithiolene chelate modulates the electronic structure and catalytic reactivity of the molybdenum centers of enzymes.

Experimental Section

Abbreviations. Tp*, hydrotris(3,5-dimethyl-1-pyrazolyl)borate; bdt, 1,2-benzenedithiolene; qdt, 2,3-quinoxalinedithiolene; tdt, 3,4-toluenedithiolene; bdtCl_2, 3,6-dichlorobenzenedithiolene; SPhMe, toluenethiolate; S_{ip}, in-plane dithiolene sulfur orbitals; S_{op}, out-of-plane dithiolene sulfur orbitals.

General. Unless otherwise stated, all reactions and manipulations were carried out under an inert atmosphere of pure dry argon by using Schlenk techniques. Spectroscopic and electrochemical samples were prepared in a glovebag under a positive pressure of argon to ensure sample integrity. Purification of organic solvents followed standard procedures. All solvents (OmniSolv and DriSolv; EM Science) were dried by distillation under nitrogen and thoroughly deoxygenated prior to use via a combination of repeated freeze−pump−thaw cycling and argon saturation. The preparation and characterization of the quinoxaline-2,3-dithiol (H_2qdt) ligand followed previous reported methods.[43−45] (Tp*)Mo^{V}O(qdt) (**4**)[19,20,41] and the related compounds (Tp*)Mo^{V}O(bdt) (**1**),[26,27] (Tp*)Mo^{V}O-(tdt) (**2**),[29] (Tp*)Mo^{V}O(bdtCl_2) (**3**),[34] and (Tp*)Mo^{V}O(SPhMe)$_2$ (**5**)[29] were prepared from (Tp*)MoOCl_2 following previously reported procedures.[19,29,34] (Tp)*MoO(qdt) was further purified under argon by a combination of multiple extraction (toluene/pentane; dichloromethane/hexane) and flash chromatographic steps (silica gel 230−400 mesh, Aldrich; eluted in binary mixtures of toluene/1,2-dichloroethane (1:1) and dichloromethane/cyclohexane (1:2) as a

(33) Helton, M. E.; Gruhn, N. E.; McNaughton, R. L.; Kirk, M. L. *Inorg. Chem.* **2000**, *39* (11), 2273−2278.
(34) Inscore, F. E.; Joshi, H. K.; McElhaney, A. E.; Enemark, J. H. *Inorg. Chim. Acta* **2002**, *331*, 246−256.
(35) McElhaney, A. E.; Inscore, F. E.; Schirlin, J. T.; Enemark, J. H. *Inorg. Chim. Acta* **2002**, *341*, 85−90.
(36) Olson, G. M.; Schultz, F. A. *Inorg. Chim. Acta* **1994**, *225* (1−2), 1−7.
(37) Lim, B. S.; Willer, M. W.; Miao, M. M.; Holm, R. H. *J. Am. Chem. Soc.* **2001**, *123* (34), 8343−8349.
(38) Peariso, K.; Chohan, B.; Carrano, C.; Kirk, M. *Inorg. Chem.* **2003**, *42* (20), 6194−6203.
(39) Kirk, M. L.; Peariso, K. *Polyhedron* **2004**, *23* (2−3), 499.
(40) Jones, R. M.; Inscore, F. E.; Hille, R.; Kirk, M. L. *Inorg. Chem.* **1999**, *38* (22), 4963−4970.
(41) Helton, M. E.; Gruhn, N. E.; McNaughton, R.; Kirk, M. L. *Inorg. Chem.* **2000**, *39* (11), 2273−2278.
(42) Johnson, M. K. *Prog. Inorg. Chem.* **2004**, *52*, 213−266.
(43) Morrison, D. C.; Furst, A. *J. Org. Chem.* **1956**, *21*, 470−471.
(44) Cummings, S. D.; Eisenberg, R. *Inorg. Chem.* **1995**, *34*, 2007−2014.
(45) Theriot, L. J.; Ganguli, K. K.; Kavarnos, S.; Bernal, I. *J. Inorg. Nucl. Chem.* **1969**, *31*, 3133−3140.

red band). The final red fraction was collected and evaporated to dryness in vacuo. The solid residue was resolvated in a minimal amount of dichloromethane, and the addition of hexane, layered on the concentrated solution (1:1), induced a deep red-brown powder to form, which was subsequently washed and dried upon collection. Highly purified samples of **4** submitted for physical characterization were obtained by a slow diffusion of *n*-pentane into a saturated dichloromethane solution. Reaction progress and purity of isolated compounds were monitored by thin-layer chromatography (silica gel 60 F_{254} plastic sheets; EM Science) and mass spectrometry. High-resolution mass spectrometry showed (Tp*)-MoO(qdt) (**4**) to have an $[M + H]^+$ experimental mass of 604.0889 with respect to the most abundant ^{98}Mo isotope (calcd: 604.0902). The reduction potential (relative to the F_c/F_c^+ couple in 1,2-dichloroethane) of (Tp*)MoO(qdt) (−487 mV) follows trends in the quasi-reversible Mo(V)/Mo(IV) couples observed for **1**−**4** in 1,2-dichloroethane.[34,35] The (Tp*)MoO(qdt) complex and other compounds investigated in this study were further identified by their characteristic IR, EPR, and UV/vis spectroscopic features.[19,20,26,27,29,34,41] The identity of the (Tp*)MoO(qdt) complex **4** was confirmed by an X-ray crystal structure analysis.

Physical Measurements. ^{1}H NMR spectra of the H_2qdt ligand (in DMSO-d_6) were obtained with a Bruker AM 500 spectrometer. Mass spectra were recorded on a JEOL HX110 high-resolution sector instrument utilizing fast atom bombardment (FAB) in 3-nitrobenzyl alcohol solutions. Cyclic voltammetry (CV) data were collected on a Bioanalytical Systems (BAS) CV-50W system with an electrochemical cell consisting of a platinum disk working electrode (1.6 mm diameter, BAS), a platinum wire counter electrode (BAS), and a NaCl saturated Ag/AgCl reference electrode (BAS). CV measurements were performed in 1,2-dichloroethane solutions (10 mL, ∼1mM, 25 °C) with 0.1−0.2 M dried tetra-*n*-butylammonium tetrafluoroborate [*n*-Bu_4N][BF_4] (Aldrich) as the supporting electrolyte. Ferrocene was utilized as an internal standard, and all potentials were referenced relative to the Fc/Fc^+ couple. IR spectra were measured on solid (KBr disks) and solution (dichloromethane between NaCl plates) samples on a Nicolet Avatar ESP 360 FT-IR spectrophotometer. Electron paramagnetic resonance (EPR) spectra at X-band frequency (∼9.1 GHz) of solution (298 K) and frozen toluene glasses (77 K) were obtained on a Bruker ESP 300 spectrometer. Electronic absorption spectra of samples solvated in 1,2-dichloroethane solutions were recorded on a Cary 300 (250−900 nm) or a modified Cary 14 (with OLIS interface, 250−2600 nm) spectrophotometer. Details of the electrochemical and spectroscopic measurements for these complexes have been described previously.[19,20,26,27,29,34,41]

X-Ray Structure Determination. Suitable crystals of the (Tp*)-MoO(qdt) (**4**) complex were obtained as dark-red blocks by slow vapor diffusion of pentane into a dichloromethane solution at room temperature. The experimental details for the X-ray crystallographic study of **4** are summarized in Table 1. The crystal was mounted on a glass fiber (in a glass capillary) in a random orientation and examined on a Bruker SMART 1000 CCD detector X-ray diffractometer at 170(2) K and a power setting of 50 kV (40 mA). The structural data presented here are shown with empirical absorption and decay corrections using the program SADABS. The structure was solved by direct methods using SHELXS in the Bruker SHELXTL (Version 5.0) software package. Refinements were performed using SHELXL, and illustrations were made using XP. Hydrogen atoms were added at idealized positions, constrained to ride on the atom to which they are bonded, and given thermal parameters equal to 1.2 or 1.5 times U_{iso} of that atom. A parameter describing extinction was included. Scattering factors and anomalous dispersion were taken from International Tables, Vol. C, Tables 4.2.6.8 and 6.1.1.4.[46,47] Selected crystallographic data and molecular structural parameters for **4** are listed in Tables 1 and 2, respectively. Further experimental details and data from the X-ray crystallographic study are given in the Supporting Information (Tables S1−S5).

Table 1. Crystal Data and Structure Refinement Parameters for (Tp*)MoO(qdt) (**4**)

empirical formula	$C_{23}H_{26}BMoN_8OS_2$	
fw	601.39	
temp	170(2) K	
wavelength	0.71073 Å	
cryst syst	triclinic	
space group	$P\bar{1}$	
unit cell dimensions	a = 9.8424(7) Å	α= 92.7560(10)°.
	b = 11.2323(8) Å	β= 98.9530(10)°.
	c = 11.9408(8) Å	γ = 104.1680(10)°.
V	1259.21(15) Å^3	
Z	2	
density (calcd)	1.586 Mg/m^3	
absorption coeff	0.721 mm^{-1}	
F(000)	614	
cryst size	0.15 × 0.10 × 0.10 mm^3	
θ range for utilized data	1.73−29.57°	
limiting indices	$-13 \le h \le 13$, $-15 \le k \le 15$, $-16 \le l \le 16$	
reflns utilized	16 848	
independent reflns	6424 [R(int) = 0.0309]	
completeness to θ = 29.57°	90.9%	
absorption correction	empirical	
max. and min. transmission	1.00 and 0.934873	
refinement method	full-matrix least-squares on F^2	
data/restraints/params	6424/0/331	
GOF on F^2	1.071	
final R indices [$I > 2\sigma(I)$]	R1 = 0.0346, wR2 = 0.0850	
R indices (all data)	R1 = 0.0490, wR2 = 0.0925	
largest diff. peak and hole	1.626 and −0.349 e·Å^{-3}	
RMS difference density	0.098 e·Å^{-3}	

Table 2. Important Mean Bond Lengths [Å] and Angles [deg] for (Tp*)MoO(qdt) (**4**), (Tp*)MoO(bdt) (**1**), and (Tp*)MoO(bdtCl$_2$) (**3**)[a]

	(**4**)	(**3**)[b]	(**1**)[c]
Mo(1)−O(1)	1.686(2)	1.679(3)	1.678(4)
Mo(1)−N(eq)	2.177(2)	2.171(3)	2.178(5)
Mo(1)−N(31)	2.348(2)	2.391(3)	2.372(4)
Mo(1)−S(eq)	2.388(7)	2.374(12)	2.373(2)
S−C	1.761(3)	1.751(4)	1.760(6)
C(2)−C(1)	1.444(4)	1.406(5)	1.395(8)
O(1)−Mo(1)−N(eq)	93.25(9)	91.73(12)	92.35(2)
N(11)−Mo(1)−N(21)	86.30(8)	86.17(11)	85.5(2)
O(1)−Mo(1)−N(31)	169.85(8)	166.79(11)	169.2(2)
N(eq)−Mo(1)−N(31)	79.42(8)	78.70(11)	79.8(2)
S(eq)−Mo(1)−N(31)	87.63(6)	88.32(8)	86.95(1)
O(1)−Mo(1)−S(eq)	99.79(7)	101.40(10)	100.95(2)
N(11)−Mo(1)−S(1)	166.68(6)	166.47(8)	167.3(1)
N(21)−Mo(1)−S(1)	93.06(6)	91.54(8)	93.7(1)
N(11)−Mo(1)−S(2)	92.55(6)	94.92(8)	92.6(1)
N(21)−Mo(1)−S(2)	167.25(6)	167.05(8)	166.1(1)
S(1)−Mo(1)−S(2)	85.14(2)	84.38(4)	85.12(6)
Mo−S(eq)−C	102.0	107.0	103.8
S(eq)−C(1)−C(2)	120.4	120.6	121.0
S···S bite distance	3.231	3.190	3.210
Mo distance from N_2S_2 plane	0.258	0.258	0.264
fold angle (θ)	29.5	6.9	21.3
θ_d ($MoS_2 \angle MoN_2$)	162.2	162.2	161.2

[a] eq refers to averaged equatorial ligand parameters. [b] Parameters taken from ref 30. [c] Parameters taken from refs 26 and 27.

Resonance Raman Spectroscopy. The instrumentation and experimental methodologies for collecting rR data on the [(Tp*)-

(46) *International Tables for Crystallography*; Kluwer Academic Publishers: Dordrecht, The Netherlands, 1995; Vol. A.
(47) *International Tables for Crystallography*; Kluwer Academic Publishers: Dordrecht, The Netherlands, 1995; Vol. C.

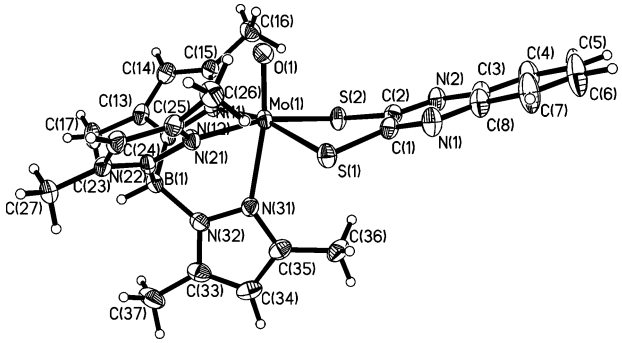

Figure 4. ORTEP drawing of (Tp*)MoO(qdt) (**4**). The atoms are drawn as 50% probability ellipsoids. H atoms have been made arbitrarily small for clarity (see Figure S2 for additional ORTEP views).

$MoO]^{2+}$ system of compounds have been discussed previously in detail.[19] A Coherent Innova 70−5 argon-ion laser (9 discrete lines, 457.9−528.7 nm) was utilized for inducing Raman scattering. The scattered radiation was dispersed onto a liquid-nitrogen-cooled 1 in. Spex Spectrum One CCD detector using a Spex 1877E triple grating monochromator with a 1800 gr/mm holographic grating at the spectrographic stage. The laser power at the sample was maintained at 90 mW in order to minimize possible photo- and thermal degradation of the samples. Solid samples were prepared as finely ground powders and dispersed in NaCl with Na_2SO_4 or $NaNO_3$ added as an internal standard. Solution Raman spectra were obtained in degassed benzene. Raman samples were sealed in NMR tubes for data collection. Relative Raman intensities and band positions for a specific vibrational mode were measured with respect to the 992.4, 1069.4, and 992 cm^{-1} bands of Na_2SO_4, $NaNO_3$, and benzene, respectively. Solution spectra were also recorded in CS_2. All Raman data were collected in a 135° backscattering geometry and scan averaged.

Normal Mode Calculations. To investigate the vibrational normal modes of **4**, a fully geometry optimization of the computational model $[(NH_3)_3MoO(qdt)]^{1+}$ was performed, followed by a harmonic vibrational frequency analysis. These calculations were carried out at the UB3LYP level using the Gaussian03 suite of programs.[48] A 6-31G** basis set was used for all atoms except Mo, where the Los Alamos effective core potentials (LANL2DZ) were used.

Results and Discussion

Structure of (Tp*)MoO(qdt). The structure of (Tp*)-MoO(qdt) (**4**) was determined by single-crystal X-ray diffraction and is presented in Figure 4. The perspective view illustrates the general atomic numbering scheme used for defining the molecular structural parameters of **4** and other related [(Tp*)Mo^{V}O(dithiolene)] complexes. Table 2 presents selected interatomic distances and bond angles for **4** and compares them to the corresponding mean geometric structural parameters of (Tp*)MoO(bdt) (**1**)[26,27] and (Tp*)MoO-($bdtCl_2$) (**3**).[34] These mononuclear six-coordinate monooxo-Mo(V) monodithiolene complexes (**1**, **3**, and **4**), in addition to the bis-thiolate (Tp*)$MoO(SPh)_2$,[29] are, to the best of our knowledge, the only known species of the (Tp*)$Mo^{V}O(SR)_2$/(Tp*)Mo^{V}O(dithiolene) system type that have been structurally characterized by single-crystal X-ray diffraction. The molecular structure of **4** revealed a distorted six-coordinate geometry, which is defined by one terminal axial oxygen, two equatorial dithiolene sulfurs, and three pyrazolyl ring nitrogens. No symmetry is crystallographically imposed on **1** by the $P\bar{1}$ space group; however, the effective point symmetry of the molybdenum center is C_S. The terminal oxo ligand and the two sulfur donor atoms of the dithiolene chelate ligand (qdt) are constrained to be mutually cis to each other by the fac stereochemistry imposed by the tridentate $(Tp^*)^-$ ligand. The bond angles about the six-coordinate Mo atom deviate from that of octahedral geometry. This is evident by the three nonlinear trans angles and as illustrated by the obtuse O−Mo−S1 = 99.82(7)° and O−Mo−S2 = 99.75(7)° cis angles. The O−Mo−S and O−Mo−N cis angles are found to be greater than 90° in all of the structurally characterized (Tp*)$MoO(S_2)$ complexes, as anticipated.[26,27,29,34] The angular distortions of the equatorial ligand donor atoms cis to a terminal oxo has been rationalized in terms of minimizing nonbonded repulsions between the filled p(π) orbitals of the donor atoms coordinated to Mo and the π-electron density in the short Mo≡O bond.[27] The rigid geometric constraints and bonding properties of the $(Tp^*)^-$ ligand minimize the cis angular distortions involving the pyrazolyl ring nitrogens coordinated to Mo. The structural parameters of the $[(Tp^*)MoO]^{2+}$core are not unusual and are in agreement with those found for other related structurally characterized oxo-Mo(V) complexes.[26,27,34,49−54] The observed Mo≡O distance (1.686(2) Å) in **4** is not significantly different from that of (Tp*)MoO(bdt) (1.678-(4) Å),[26,27] (Tp*)$MoO(bdtCl_2)$ (1.679(3) Å),[34] or (Tp*)MoO-$(SPh)_2$ (1.676(4) Å).[29] The terminal oxo ligand, as expected, exerts a trans influence, lengthening the Mo−N31 distance (2.348(2) Å) by 0.177 Å relative to Mo−N21 (2.171(2) Å) and 0.164 Å relative to Mo−N11 (2.184(2) Å). The Mo−N31 distance (2.348(2) Å) observed in **4** is somewhat shorter than in **1** and **3**. The average Mo−S distance (2.388 Å) in **4** is lengthened (∼0.015 Å (7σ)) compared to that observed in **1** (2.373(2) Å). The mean O−Mo−S angle in **4** (99.8°) is

(48) Frisch, M. J.; Trucks, G. W.; Schlegel, H. B.; Scuseria, G. E.; Robb, M. A.; Cheeseman, J. R.; Montgomery, J. A., Jr.; Vreven, T.; Kudin, K. N.; Burant, J. C.; Millam, J. M.; Iyengar, S. S.; Tomasi, J.; Barone, V.; Mennucci, B.; Cossi, M.; Scalmani, G.; Rega, N.; Petersson, G. A.; Nakatsuji, H.; Hada, M.; Ehara, M.; Toyota, K.; Fukuda, R.; Hasegawa, J.; Ishida, M.; Nakajima, T.; Honda, Y.; Kitao, O.; Nakai, H.; Klene, M.; Li, X.; Knox, J. E.; Hratchian, H. P.; Cross, J. B.; Bakken, V.; Adamo, C.; Jaramillo, J.; Gomperts, R.; Stratmann, R. E.; Yazyev, O.; Austin, A. J.; Cammi, R.; Pomelli, C.; Ochterski, J. W.; Ayala, P. Y.; Morokuma, K.; Voth, G. A.; Salvador, P.; Dannenberg, J. J.; Zakrzewski, V. G.; Dapprich, S.; Daniels, A. D.; Strain, M. C.; Farkas, O.; Malick, D. K.; Rabuck, A. D.; Raghavachari, K.; Foresman, J. B.; Ortiz, J. V.; Cui, Q.; Baboul, A. G.; Clifford, S.; Cioslowski, J.; Stefanov, B. B.; Liu, G.; Liashenko, A.; Piskorz, P.; Komaromi, I.; Martin, R. L.; Fox, D. J.; Keith, T.; Al-Laham, M. A.; Peng, C. Y.; Nanayakkara, A.; Challacombe, M.; Gill, P. M. W.; Johnson, B.; Chen, W.; Wong, M. W.; Gonzalez, C.; Pople, J. A. *Gaussian 03*, revision B.02; Gaussian, Inc.: Wallingford, CT, 2004.

(49) Roberts, S. A.; Ortega, R. B.; Zolg, L. M.; Cleland, W. E.; Enemark, J. H. *Acta Crystallogr.* **1987**, *C43*, 51−53.

(50) Kipke, C. A.; Cleland, W. E.; Roberts, S. A.; Enemark, J. H. *Acta Crystallogr.* **1989**, *C45*, 870−872.

(51) Chang, C.-S. J.; Pecci, T. J.; Carducci, M. D.; Enemark, J. H. *Inorg. Chem.* **1993**, *32* (19), 4106−4110.

(52) Chang, C.-S. J.; Pecci, T. J.; Carducci, M. D.; Enemark, J. H. *Acta Crystallogr.* **1992**, *C48*, 1096−1097.

(53) Basu, P.; Bruck, M. A.; Li, Z.; Dhawan, I. K.; Enemark, J. H. *Inorg. Chem.* **1995**, *34* (1), 405−407.

(54) Lincoln, S. E.; Koch, S. A. *Inorg. Chem.* **1986**, *25*, 1594−1602.

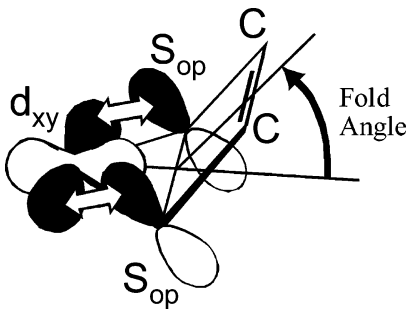

Figure 5. Graphical depiction of the fold angle in metallodithiolenes such as Tp*MoO(qdt) (**4**). Note that, as the magnitude of the fold angle increases, the overlap between out-of-plane dithiolene sulfur p orbitals (S_{op}) and the Mo d_{xy} redox-active molecular orbital increases.

slightly smaller than in **1** (100.9°) or **3** (101.4°) (see Table 2). The O−Mo−N cis angles in each of these complexes are observed to decrease slightly relative to an increase in the mean O−Mo−S angle, which tilts the N_2S_2 least-squares plane toward the $\pm z$ axes (projected along the Mo≡O bond vector), respectively. The trans O−Mo−N31 angle is distorted the least in **4**, which possesses the smallest mean O−Mo−S angle within this series of compounds. These angular deviations within the equatorial N_2S_2 planes of **4**, **3**, and **1** appear to be invariant, as reflected by the nearly constant dihedral angle ($\theta_d \approx 162°$) measured between the midpoint of the MoS_2 and MoN_2 planes in these six-coordinate systems. The result of these distortions in the cis angles ($O-Mo-L_{eq} > 90°$) is that the molybdenum atom in **4** is displaced ~0.258 Å above the N_2S_2 least-squares plane in the direction of the apical oxo ligand. This perpendicular displacement is slightly less than that observed for **1** (0.264 Å). The S−Mo−S angle in **4** is 85.14(2)° and nearly identical to that observed for **1** (85.12(6)°). However, due to the elongated Mo−S bond lengths in **4**, the measured S···S nonbonded contact distance (3.231 Å) is slightly greater than that observed for **1** (3.210 Å). This metric parameter is somewhat smaller than the estimated van der Waals contact of 3.7 Å and the nominal nonbonded S···S contact of 3.4 Å in the (Tp*)MoO(SPh)$_2$ complex ($Mo-S_{avg} = 2.382$ Å, S−Mo−S = 90.98°),[29] which underscores the unique geometric constraints imposed by the dithiolene chelate ring coordinated to Mo in **1**−**4**. The other mean nonbonded contact distances in **4** involving the atoms defining the inner coordination sphere about Mo are also slightly less than their estimated van der Waals contacts, as was the case for **1** and **3**.

The qdt ligand in **4** is approximately planar but folded up toward the terminal oxo ligand (Figure 5). The fold angle[34,44] between the dithiolene (S−C═C−S) least-squares plane and the S−Mo−S plane along the line of intersection containing the S···S atoms is 29.5° This is somewhat greater than the 21.3(1)° fold angle measured for **1**.[27] Originally, the deformation in **1** was attributed to a steric (nonbonded) interaction between the C36 methyl group of the trans N31 pyrazolyl ring and the chelate ring C1 and C2 atoms.[27] The C36···C1 and C36···C2 contact distances (3.57 and 3.58 Å, respectively), in **1** are less than the estimated van der Waals contact of 3.72 Å between a methyl group and an aromatic ring.[27] However, in **4**, the C36···C1 and C36···C2 contact distances of 3.797 and 3.752 Å in **4** are substantially larger than those reported for **1** and **3**. A crystal packing analysis of **4** revealed no additional interactions with neighboring molecules (Figure S1). The C36···C1 and C36···C2 contact distances illustrate an interesting point regarding the symmetry of **4** compared to **1**, where the O−Mo−N31 angle is 169.2° and the C36···C1 and C36···C2 distances are indistinguishable. In **4**, a similar O−Mo−N31 angle is observed (169.85°) but the C36···C1 and C36···C2 contact distances differ by 0.045 Å. These data are consistent with the N31 pyrazolyl ring of **4** deviating slightly from the mirror plane (see Figure S2; where C36 is canted toward C2), implying a lower symmetry (C_1) for **4**. However, the difference in nonbonded contacts is sufficiently small that the effective point symmetry of **4** is still treated as effective C_S. More recently, the importance of electronic effects in the observed fold angle have been considered.[55,56] It has been shown that larger fold angles occur when the d_{xy} orbital is empty and can accept electron density from the filled symmetric S p orbitals, as shown in Figure 5. For d^1 systems, such as **4**, intermediate fold angles occur that appear to be sensitive to the electron-donating (withdrawing) ability of the particular dithiolene ligand. The metric parameters of the MoS_2C_2 chelate ring are also of particular interest. Both complexes (**1** and **4**) have nearly identical S−C bond lengths of 1.76 Å that are within the normal range reported for oxo-Mo(V) dithiolene systems.[34,37,57−59] However, the C1−C2 distance of 1.444(4) Å for **4** is larger than the corresponding bond length of 1.395(8) Å in **1** (Table 2). The dimensions of the qdt ligand in **4** are similar to those which have been reported for $[Mo(qdt)_3]^{2-/1-}$, $[Ni(qdt)_2]^{2-}$, and $[Cu(qdt)_2]^{2-/1-}$.[60−62] Therefore, the longer C1−C2 bond length observed in **4** relative to **1** appears to be a structural feature characteristic of transition metal complexes possessing the qdt ligand, which reflects the electron-withdrawing properties of the heterocyclic nitrogen atoms of the pyrazine ring that is fused directly to the dithiolene chelate. The dithiolene chelate ring fragment in these (Tp*)MoO(dithiolene) complexes also exhibits a significant structural variation with respect to the Mo−S−C angle (Table 2). The mean Mo−S−C angle of 102.0° in **4** is smaller than that measured for **1** (103.8°) and **3** (107.0°).

The results of the X-ray crystallographic studies of **4** and those reported previously for **1**[26,27] and **3**[34] are important for understanding remote and second coordination sphere ligand

(55) Joshi, H. K.; F. E. I.; Schirlin, J. T.; Dhawan, I. K.; Carducci, M. D.; Bill, T. G.; Enemark, J. H. *Inorg. Chim. Acta* **2002**, *337*, 275−286.
(56) Cooney, J. A.; M. A. C.; Gruhn, N. E.; Joshi, H. K.; Enemark, J. H. *Inorg. Chem.* **2004**, *43*, 8110−8118.
(57) Boyde, S.; Ellis, S. R.; Garner, C. D.; Clegg, W. *J. Chem. Soc., Chem. Commun.* **1986**, (20), 1541−1543.
(58) Lim, B. S.; Donahue, J. P.; Holm, R. H. *Inorg. Chem.* **2000**, *39* (2), 263−273.
(59) Donahue, J. P.; Lorber, C.; Norlander, E.; Holm, R. H. *J. Am. Chem. Soc.* **1998**, *120*, 3259−3260.
(60) Boyde, S.; Garner, C. D.; Clegg, W. *J. Chem. Soc., Dalton Trans.* **1987**, (5), 1083−1087.
(61) Boyde, S.; Garner, C. D.; Enemark, J. H.; Bruck, M. A.; Kristofzski, J. G. *J. Chem. Soc., Dalton Trans.* **1987**, 2267−2271.
(62) Pignedoli, A.; Peyronel, G.; Antolini, L. *Acta Crystallogr.* **1974**, *B30*, 2181−2185.

effects on the geometric and electronic structures of oxo-Mo mono-dithiolene systems. The key feature obtained from comparing the molecular parameters of **4** and **1** is that the coordination geometries are very similar, suggesting that remote effects resulting from ancillary variations to the dithiolene chelate do not induce significant structural changes involving the inner coordination about the molybdenum atom. These results are consistent with structures of oxo-Mo-dithiolenes obtained by X-ray and EXAFS that show no appreciable differences in the Mo−S bond distance.[37,57−59,63,64] However, as these remote effects involve EXAFS indiscernible changes, their contributions to the overall geometric structure in the protein active sites during catalytic turnover can only be elucidated directly by high-resolution X-ray crystallography as it becomes available. This is important, as the structures of **4**, **3**, and **1** have revealed that remote ligand effects do induce substantial changes in the molecule beyond the first coordination sphere, and this is evident by perturbations to the fold angle (θ) and Mo−S−C angles of the ene-1,2-dithiolene chelate. These outer-sphere structural variations may play an important role in fine-tuning the electronic properties of oxomolybdenum dithiolenes. Therefore, it remains to be determined whether the electronic structure differences observed between these complexes are due exclusively to the electron-donating capabilities of the dithiolene ligand S donor atoms, as suggested by the relatively invariant inner coordination sphere metric parameters, or are also a consequence of structural variations which affect the orientation of those orbitals involved in Mo−S interactions.

Vibrational and Resonance Raman Spectra. The solid-state infrared spectrum of **4** exhibited an intense peak at 940 cm^{-1} similar to that reported for a variety of complexes possessing the $[(Tp^*)Mo^VO]^{2+}$moiety.[29,65−69] This intense feature is easily assigned as the Mo≡O stretching mode due to its high oscillator strength and the fact that it is observed in the IR and often the Raman spectra of other mono-oxomolybdenum dithiolenes. The Mo≡O stretch is observed at a higher frequency in **4** than in the related **1** (932 cm^{-1}), **2** (926 cm^{-1}), and **3** (934 cm^{-1}).[19,26,29,34] Typically, variation in the high-frequency Mo≡O stretch among similar oxo-molybdenum compounds is relatively small, and this is consistent with the nearly invariant inner-coordination sphere metric parameters observed for these complexes. However, these small vibrational differences are discernible, which suggests that the relatively rigid $[(Tp^*)MoO]^{2+}$ core is sensitive to the electron-donor/withdrawing capabilities of the ligands ancillary to this core. As such, the shift in the Mo≡O stretch to higher frequency in **4** relative to **1** is consistent with the electron-withdrawing nature of the quinoxaline ring, which would be expected to enhance O_{oxo}-(2p)−Mo($d_{xz,yz}$) π-bonding by a reduction in dithiolene sulfur charge donated to the metal from the charge deficient qdt^{2-} dithiolene ligand.[70,71]

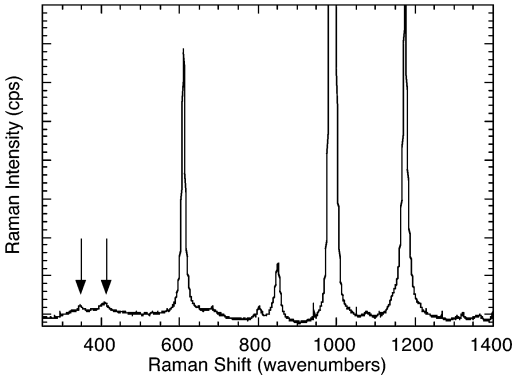

Figure 6. The room-temperature resonance Raman spectrum of (Tp*)-MoO(qdt) (**4**) in benzene at 514.5 nm excitation (90 mW). Arrows indicate Raman bands originating from Tp*MoO(qdt) at 348 and 407 cm^{-1}.

The room-temperature solution Raman spectrum of **4** (Figure 6) yields Raman-active modes intrinsic to **4** at 348 and 407 cm^{-1} using 514.5 nm excitation. The 940 cm^{-1} Mo≡O stretch, observed in the IR, is not observed in the Raman spectrum of **4** using 514.5 cm^{-1} excitation. Generally, one to three bands have been observed in the 300−400 cm^{-1} region for metallo-dithiolene complexes and these have collectively been assigned as either Mo−S stretching or bending vibrations,[19] with the most-intense feature assigned as the Mo−S symmetric stretch.[72−77] Similar vibrational modes have been observed in this region for the pyranopterin molybdenum enzymes SO and DMSO reductase, which have also been tentatively assigned as Mo−S stretching modes.[42]

The absorption band at 19 100 cm^{-1} (ϵ = 1050 M^{-1} cm^{-1}) in **4** has previously been assigned as a $S_{ip} \rightarrow Mo(d_{xy})$ charge transfer.[19] The intensity of this charge-transfer transition reflects the degree of S_{ip}−Mo(d_{xy}) orbital mixing, which has been suggested to be the key dithiolene−Mo interaction responsible for coupling the active sites of pyranopterin Mo enzymes into efficient hole superexchange pathways for electron-transfer regeneration. This assignment was facilitated by a combination of electronic absorption and MCD spectroscopies and an overall spectral similarity to the related **1** and **2**.[19] The rR excitation profiles constructed previously for **1** and **2** have provided definitive assignments for all of

(63) Musgrave, K. B.; Donahue, J. P.; Lorber, C.; Holm, R. H.; Hedman, B.; Hodgson, K. O. *J. Am. Chem. Soc.* **1999**, *121* (44), 10297−10307.
(64) Musgrave, K. B.; Lim, B. S.; Sung, K. M.; Holm, R. H.; Hedman, B.; Hodgson, K. O. *Inorg. Chem.* **2000**, *39* (23), 5238.
(65) Backes, G.; Enemark, J. H.; Loehr, T. M. *Inorg. Chem.* **1991**, *30* (8), 1839−1842.
(66) Chang, C.-S. J.; Collison, D.; Mabbs, F. E.; Enemark, J. H. *Inorg. Chem.* **1990**, *29* (12), 2261−2267.
(67) Chang, C.-S. J.; Enemark, J. H. *Inorg. Chem.* **1991**, *30*, 683−688.
(68) Lincoln, S. E.; Loehr, T. *Inorg. Chem.* **1990**, *29*, 1907−1915.
(69) Nipales, N. S.; Westmoreland, T. D. *Inorg. Chem.* **1995**, *34*, 3374−3377.
(70) Ellis, S. R.; Collison, D.; Garner, C. D. *J. Chem. Soc., Dalton Trans.* **1989**, (3), 413−417.
(71) Wang, K.; McConnachie, J. M.; Stiefel, E. I. *Inorg. Chem.* **1999**, *38* (19), 4334−4341.
(72) Subramanian, P.; Burgmayer, S.; Richards, S.; Szalai, V.; Spiro, T. G. *Inorg. Chem.* **1990**, *29*, 3849−3853.
(73) Oku, H.; Ueyama, N.; Nakamura, A. *Inorg. Chem.* **1995**, *34* (14), 3667−3676.
(74) Oku, H.; Ueyama, N.; Kondo, M.; Nakamura, A. *Inorg. Chem.* **1994**, *33* (2), 209−216.
(75) McNaughton, R. L.; Helton, M. E.; Rubie, N. D.; Kirk, M. L. *Inorg. Chem.* **2000**, *39*, 4386−4387.
(76) Clark, R. J. H.; Turtle, P. C. *J. Chem. Soc., Dalton Trans.* **1978**, (12), 1714−1721.
(77) Kilpatrick, L.; Rajagopalan, K. V.; Hilton, J.; Bastian, N. R.; Stiefel, E. I.; Pilato, R. S.; Spiro, T. G. *Biochemistry* **1995**, *34* (9), 3032−3039.

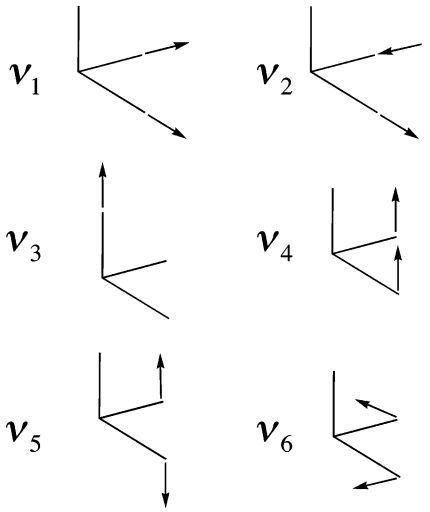

Figure 7. The $3N - 6$ symmetry coordinates for the MoO(S−S) core. The coordinate framework shown with the *z* axis directed along the Mo≡O bond vector and coincident with the mirror plane requires rotation of the axes system from that normally defined in C_S point group symmetry. The Mo $d_{x^2-y^2}$ orbital is projected in the equatorial plane along the Mo−S bond vectors and the redox-active singly occupied HOMO (primarily Mo d_{xy} in character) bisects the equatorial chelated atoms (MoS_2 and MoN_2).

the low-energy S → Mo charge-transfer transitions in these complexes in addition to providing considerable insight into their electronic structures and metal−ligand bonding schemes.[19] The strong axial oxo ligand field in the presence of a moderate equatorial ligand field determines the ordering, relative energies, and spatial orientation of the Mo d orbitals, and the spectroscopic innocence of the Tp* ligand results in all LMCT transitions below ~25 000 cm^{-1} in (Tp*)MoO(dithiolene) compounds being S → Mo in origin.[19,78] This has provided the basis for using a simple four-atom chromophore model to understand the rR spectra of (Tp*)MoO(dithiolene) complexes, and the resulting $3N - 6 = 6$ symmetry coordinates are depicted in Figure 7.[18,19] Since (Tp*)MoO(dithiolene) complexes possess effective C_s symmetry, excited-state distortions are expected to occur along the four totally symmetric modes (ν_1, ν_3, ν_4, ν_6,), and these are the modes that will be resonantly enhanced by an Albrecht A-term mechanism. However, excitation into the S_{ip} → Mo(d_{xy}) charge-transfer band of **1**, **2**, and **4** results in resonance enhancement along only two of these coordinates, ν_1 and ν_6, which represent distortions along the Mo−S bonds in the plane orthogonal to the Mo≡O bond. The ν_3 Mo≡O stretching mode is resonantly enhanced with excitation into the higher energy S_{op} → Mo($d_{xz,yz}$) charge-transfer bands of **1** and **2** with a large reduction in the enhancement of ν_1 and ν_6.[18,19] This is a direct result of the dominant $O_{oxo}(2p)$−Mo($d_{xz,yz}$) π^* antibonding interactions in this orbital that result in a large excited-state distortion along the ν_3 Mo≡O mode. Problems with background fluorescence in **4** have thus far precluded the observation of the ν_3 mode in this compound. The ν_4 mode has not been observed in any of the (Tp*)MoO(dithiolene) compounds, and this is likely due to the lack of an appreciable excited-state distortion along this coordinate. The anticipated weak intensity, coupled with its low frequency, likely results in ν_4 being obscured by the intense Rayleigh line. A key observation of particular importance regarding the protein active sites is that, in contrast to the low number of vibrational modes observed in well-characterized oxomolybdenum dithiolene model compounds, the rR spectra of the DMSO reductase[25,77,79] from *R. sphaeroides* and recombinant human SO[25] possess much more complicated spectra and exhibit multiple vibrational modes between 200 and 1700 cm^{-1} that are apparently resonantly enhanced. Therefore, determining which vibrational modes are *intrinsic* to the oxomolybdenum dithiolene core, in addition to determining their normal mode character, is of considerable importance in developing a comprehensive understanding of enzyme spectra and pyranopterin dithiolene contributions to reactivity.[42]

The observation of an in-plane bending mode in the 300−400 cm^{-1} Mo−S stretching region is counterintuitive, as the energy required to stretch a 3-center S−Mo−S bond along ν_1 should be greater than that required to bend it along the ν_6 coordinate.[80] The origin of the high frequency for the ν_6 mode may be attributed to the nature of dithiolene chelate, as the "stiffness" of the chelate ring is anticipated to impede the free S···S motion associated with the symmetric bend. This constrained movement translates into a larger force constant that should result in the ν_6 S−Mo−S bending mode being shifted to higher frequency. Interestingly the assignment of ν_6 in square planar $[NEt_4]_2[Ni(mnt)]$ ($\nu_6 \approx 180$ cm^{-1}) is found to be considerably lower in frequency than that observed in (Tp*)MoO(dithiolene) compounds.[42] However, the frequency of the ν_6 symmetric bend increases and is only ~20 cm^{-1} lower than the ν_1 symmetric stretch, in metallobis(dithiolenes) which possess highly conjugated dithiolenes (i.e., $dmit^{2-}$).[42] This suggests that electronic and geometric components of a coordinated dithiolene ligand can conspire to affect the nature of key in-plane Mo−S normal modes, influencing the observed vibrational frequencies and normal mode compositions. Therefore, considerable mode mixing between the totally symmetric in-plane ν_1 and ν_6 modes may be anticipated as a result of the small experimental energy separation ($\Delta\nu_{1,6} \cong 60$ cm^{-1} for **4**, $\Delta\nu_{1,6} \cong 30$ cm^{-1} for **1**) observed for these modes in oxomolybdenum-mono(dithiolenes).

We have investigated the potential for vibrational mode mixing using a vibrational frequency analysis within the Gaussian03 suite of programs in order to probe the nature of the vibrational normal modes in $[(NH_3)_3MoO(qdt)]^{1+}$, a computational model for **4** where the tris-pyrazolylborate ligand has been effectively modeled by three coordinated amine donors. It is clear that extensive mode mixing occurs and the true vibrational normal modes may best be described as symmetry-adapted linear combinations of the original ν_1 and ν_6 symmetry coordinates, and these are shown in Figure

(78) Carducci, M.; Brown, C.; Solomon, E.; Enemark, J. *J. Am. Chem. Soc.* **1994**, *116* (26), 11856−11868.

(79) Gruber, S.; Kilpatrick, L.; Bastian, N. R.; Rajagopalan, K. V.; Spiro, T. G. *J. Am. Chem. Soc.* **1990**, *112* (22), 8179−8180.

(80) (Tp*)MoO(1,3-propanedithiolene) exhibited two vibrational bands (350.4 and 272.4 cm^{-1}) in the Mo−S region that are enhanced relative to the MoO mode (928.8 cm^{-1}) with excitation into the absorption band observed at ~528−457 nm.

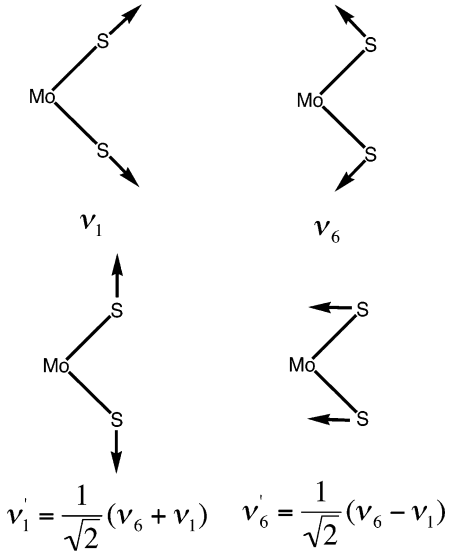

Figure 8. Linear combination of symmetry coordinates, ν_1 and ν_6, and their combination to form normal modes, ν'_1 and ν'_6.

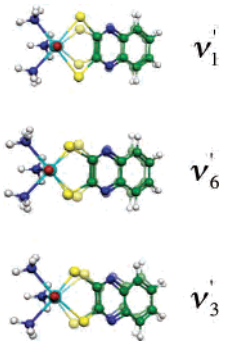

Figure 9. Calculated vibrational modes for select low-frequency vibrations in $[(NH_3)MoO(qdt)]^{1+}$. The images overlay the displacements of the atoms in the model at the extrema of their vibrational motion. The calculated frequencies for this model are 352 (ν'_1), 396 (ν'_6), and 385 (ν'_3) cm^{-1}.

8. The calculated frequencies for this model are 352 (ν'_1), 385 (ν'_3), and 396 cm^{-1} (ν'_6) (Figure 9). These calculated frequencies are in excellent agreement with the experimental data and allow us to assign the 348 and 407 cm^{-1} modes of **4** as ν'_1 and ν'_6, respectively. In support of this assignment, the rR spectrum of (Tp*)MoO(SPhMe)$_2$, which possesses two monodentate thiolate ligands in the equatorial plane, shows only a single vibrational mode at 399 cm^{-1} that most likely results from excited-state distortions that occur primarily along a single Mo−S stretching coordinate (i.e., ν_1). The ν_6 in-plane bending mode of (Tp*)MoO(SPhMe)$_2$ is likely shifted to considerably lower frequency and hence not observed in the rR spectrum because it can no longer effectively couple to excited-state distortions resulting from the low-energy CT excitations.[80,81] Therefore, the observed differences in the low-frequency region of the rR spectra for (Tp*)MoO(SR)$_2$ and (Tp*)MoO(dithiolene) complexes underscore the unique differences between these two different types of sulfur donor ligands.

Summary and Implications for Sulfite Oxidase

The X-ray and rR results presented here for **1** and **4** provide a simple platform for understanding the key electronic structure differences observed between these two oxomolybdenum-mono(dithiolenes). The X-ray structure of **4** is very similar to that of **1**, and this indicates that the significant differences observed in their reduction potentials and electronic spectra are primarily a function of the substantial differences in the electron-donating ability of the coordinated dithiolene. In contrast to the large differences in reduction potential and electronic structure previously observed between **1** and **4**,[41] these compounds possess very similar MoO(dithiolene) core vibrational frequencies and normal modes descriptions, and this is consistent with their very similar structural parameters. Both compounds exhibit two in-plane Mo−S vibrations which are resonantly enhanced with excitation into the low-energy $S_{ip} \rightarrow Mo(d_{xy})$ charge-transfer band.[18,19] Therefore, we suggest that two similar low-frequency vibrational modes, associated with a single coordinated dithiolene, may also be observed in reduced forms of SO. However, differences between the enzyme and Tp*MoO(dithiolene) model vibrational structure may be anticipated due to kinematic coupling and the presence of lower site symmetry at the active site of the protein.

Presently, there are no rR data available for SO_{red}; however, rR data for the fully oxidized molybdenum domain (SO_{ox}) in the wild-type and C207S recombinant human SO revealed two Mo=O stretching modes and two low-frequency modes that were assigned to the coordinated cysteine residue, a Mo−S_{cys} stretch (362 cm^{-1}) and S_{cys}-C−C bend (289 cm^{-1}).[25,42] Another low-frequency mode is observed in the His-tagged human SO protein at 416 cm^{-1}, but this vibration has not been assigned.[42] Interestingly, no Mo−S stretching modes associated with the dithiolene chelate were suggested to be coupled with the lowest-energy CT absorption band in SO_{ox}.[25,42] The present study reveals that Mo−$S_{dithiolene}$ vibrational modes are clearly observable in the rR spectra of structurally characterized oxomolybdenum-mono(dithiolene) compounds. These results, coupled with recent bonding calculations on the oxidized SO_{ox} site,[82] suggest that a reinvestigation of the low-frequency enzyme spectra may be warranted. Finally, the observation of two, formally 3-center S−Mo−S, vibrational modes in the 300−400 cm^{-1} Mo−S stretching region may be of fundamental importance for understanding the electron-transfer reactions of molybdenum enzymes, such as sulfite oxidase, during catalysis. The ν_1' vibration involves motion along the dithiolene S···S coordinate; thus, the electron density between these two atoms should be enhanced at the extreme of the vibration amplitude that minimizes the S···S distance. The formally d_{xy} redox orbital possesses a lobe that bisects this dithiolene S···S vector, providing a mechanism for dynamically enhancing Mo−$S_{dithiolene}$ overlap and vibronically coupling the pyranopterin dithiolene into hole superexchange pathways for electron-transfer regeneration of the SO_{ox} site. In effect, the nature of the normal modes can affect the time-

(81) Dr. Frank E. Inscore, Ph.D. dissertation, The University of New Mexico, April 2000.
(82) McNaughton, R. L.; Helton, M. E.; Cosper, M. M.; Enemark, J. H.; Kirk, M. L. *Inorg. Chem.* **2004**, *43* (5), 1625.

dependence of their composite superposition, with larger amplitudes along ν_1' resulting in stronger pseudo-σ Mo−S interactions with a decrease in the S···S vector. Such nonequilibrium structures may affect the nature of the electronic coupling matrix element (H_{ab}) in a time-dependent fashion to enhance enzymatic electron transfer. The time dependence of H_{ab} is expected to be additionally modulated by changes in the fold angle between the MoS_2 plane and the S_2C_2 plane of the dithiolene, which has been shown to be sensitive to the overall electronic structure of the metal-dithiolene moiety.[34,83]

Acknowledgment. The X-ray diffraction studies were carried out using the facilities of the Molecular Structure Laboratory, Department of Chemistry, University of Arizona under the direction of Dr. Michael Carducci; electrochemistry was performed by Anne McElhaney at the University of Arizona; mass spectra were recorded at the University of Arizona Mass Spectrometry Facility under Dr. Arpad Somogyi; EPR studies were carried out under the direction of Dr. Arnold Raitsimring at the University of Arizona. The authors wish to thank Dr. J. Jon A. Cooney for helpful insights and Dr. Partha Basu for the synthesis of (Tp*)MoO(SPhMe)$_2$. We gratefully acknowledge support by the National Institutes of Health (Grant No. GM-37773 to J.H.E. and Grant No. GM-057378 to M.L.K.).

Supporting Information Available: X-ray crystallographic files in CIF format and additional materials. This material is available free of charge via the Internet at http://pubs.acs.org.

IC0506815

(83) Joshi, H. K.; Cooney, J. J. A.; Inscore, F. E.; Gruhn, N. E.; Lichtenberger, D. L.; Enemark, J. H. *Proc. Natl. Acad. Sci. U.S.A.* **2003**, *100* (7), 3719.